Electronic Supplementary Information

Enhancing NO_2 Detection Ability of Surface Acoustic Wave Sensors with ZnO-Decorated N-doped Porous Carbon Nanosheets

Xue Li [a], Yuan Feng [a], Haifeng Lv [a], Junjie Shi [b], Yuanjun Guo [a*], Sean Li [b*] and Xiaotao Zu [a*]

[a] School of Physics, University of Electronic Science and Technology of China, Chengdu, 610054, P. R. China.

[b] School of Materials Science and Engineering, University of New South Wales, Sydney, NSW, Australia.

[*] Corresponding author E-mail: guoyuanjun@uestc.edu.cn; sean.li@unsw.edu.au; xtzu@uestc.edu.cn

1. Experimental section

1.1. SAW device

The SAW device consisted of Aluminum interdigital transducers (IDTs, 30 pairs) and reflection gratings (100 pairs), which were stamped on ST-cut quartz with excellent temperature stability. Their roles were to generate/receive the wave signal and operate at a center frequency of about 201 MHz. The aperture and the period of the IDTs were 3 mm and 16 μm, respectively. Figure S1a depicts the schematic illustration of the as-designed SAW device.

1.2. Gas sensing test

The fabricated SAW sensor was mounted in a glassy 20 L chamber, and connected with a voltage power (KEYSIGHT E3631A), a source meter (Keithely-2400), and a frequency counter (Agilent 53210A), as illustrated in Figure S1b. The operation condition was set at a temperature of 25°C and a relative humidity of 32%, otherwise controlled by a humidifier (GM1363) and some desiccants to regulate the variation of temperature and humidity. To accurately measure the experimental data, a 200 mL high-precision gas-tight syringe (Hamilton 1000) was applied to inject the targeted gases into the testing chamber. All of these targeted gases (e.g., dry H_2S, NH_3, NO_2, H_2, etc.) were directly collected from the cylinders. The different concentrations of NO_2 gas (1, 10, 20, 50, 100, 200 ppm) were controlled by adjusting the injected gas volumes such as 1, 10, 20, 50, 100, 200 ml. Dry air, controlled by a mass flow controller (MFC), was purged into the test gas chamber to maintain a constant baseline.

1.3. Materials

Calcium gluconate ($C_{12}H_{22}O_{14}{\cdot}Ca{\cdot}H_2O$, 99.0%) and zinc acetate ($C_4H_6O_4Zn{\cdot}_2H_2O$, 99.0%) were purchased from Aladdin Ltd (Chengdu, China). hydrochloric acid (HCl, 99.0%), and ethanol (C_2H_6O, 99.0%) were purchased from Kelong Chemical Regent Factory (Chengdu, China). Standard H_2S (2 vol%), NH_3 (2 vol%), NO_2 (2 vol%), H_2 (2 vol%), CH_2Cl_2 (2 vol%), and C_6H_{14} (2 vol%) gases in dry air were purchased from the National Institute of Measurement and Testing Technology, China. The ultrapure water used throughout all experiments was purified through a Millipore system. All reagents were analytical reagent grade without further purification.

1.4. Preparation of N-PCNs

Calcium gluconate was annealed for one hour at the temperature of 220 °C. The resultant brown foam-like sample was further pyrolyzed for two hours at the temperature of 800 °C in the N_2 atmosphere. After the reaction was completed and cooled, the black carbon nanosheet foam was obtained. Subsequently, the sample was etched by 2M hydrochloric acid and washed repeatedly via deionized water until the PH≈7, further to remove calcium components and other impurities. Finally, the thoroughly dry black powder was the target product of N-PCNs.[1]

1.5. Preparation of ZnO@N-PCNs

The as-obtained N-PCNs were dispersed into 30 ml of zinc acetate ethyl alcohol solution to make the loading content of ZnO is 30%, stirred overnight, and dried for 12 h at 100 °C to evaporate the solvent. The as-obtained zinc-contained N-PCNs were annealed for two hours at the temperature of 450 °C. After cooling, the black product was ZnO@N-PCNs. Weighing 10 mg of the ZnO@N-PCNs dispersed in 1 ml of ethyl alcohol and followed by treating under an ultrasonic condition for twenty minutes to form a homogeneous solution. Then, the synthetic ink was drop-coated onto the SAW sensing area and baked for several minutes to form the ZnO@N-PCNs sensitive layer.

1.6. Material characterizations

The structures of the N-PCNs and ZnO@N-PCNs were obtained by X-ray powder diffraction (XRD) patterns on a Bruker AXS D8 Advance X-ray diffractometer operating at 50 kV and 60 mA with a Cu Kα irradiation source (λ = 1.5418 Å). The elements and morphologies were examined by using energy-dispersive X-ray spectroscopy (EDS), scanning electron microscopy (SEM), and transmission electron microscopy (TEM). Functional groups and the surface chemistry of the samples were analyzed by using Fourier-transform infrared spectroscopy (FTIR) and a confocal Raman microscope (488 nm). Other material characterizations included UV-visible diffuse reflectance spectra (UV-vis), X-ray photoelectron spectroscopy (XPS), and photoluminescence (PL). The specific surface area and pore-size distribution of the sample were measured by the N_2 gas adsorption/desorption isotherm. Besides, some adsorption models were constructed by utilizing the density functional theory (DFT), and the relevant adsorption energies were also calculated.

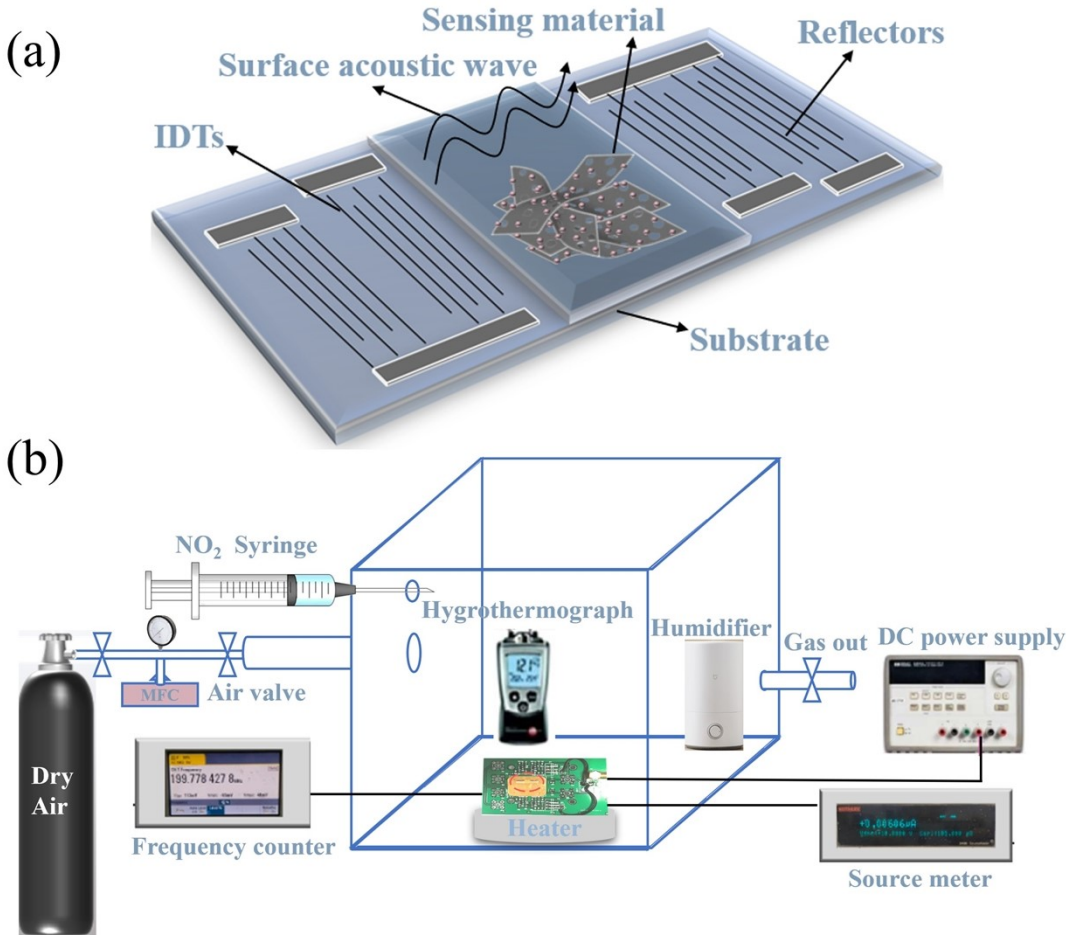

Figure S1. (a) Simple diagram of a SAW device; (b) The equipped illustration of the experimental gas sensing test.

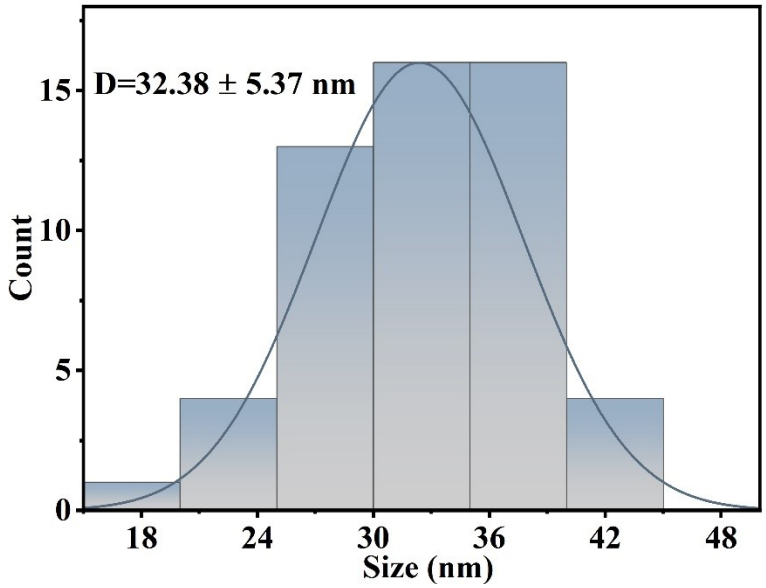

Figure S2. Particle size distribution of ZnO nanoparticles.

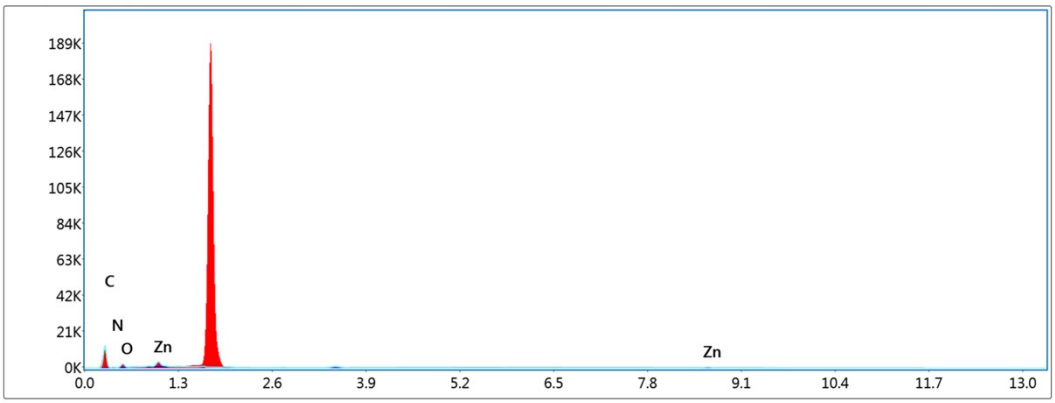

Figure S3. EDX spectrum of the ZnO@N-PCNs.

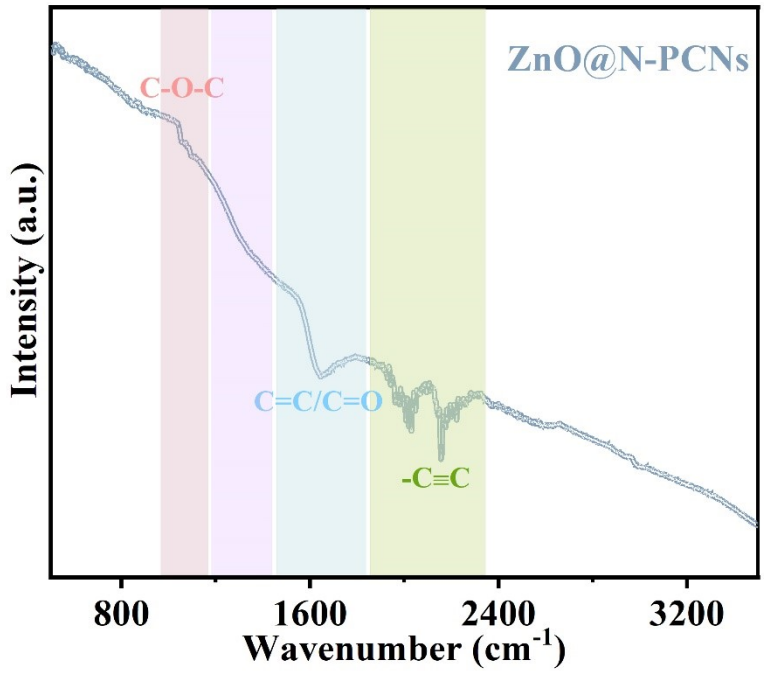

Figure S4. The FTIR spectra of ZnO@N-PCNs.

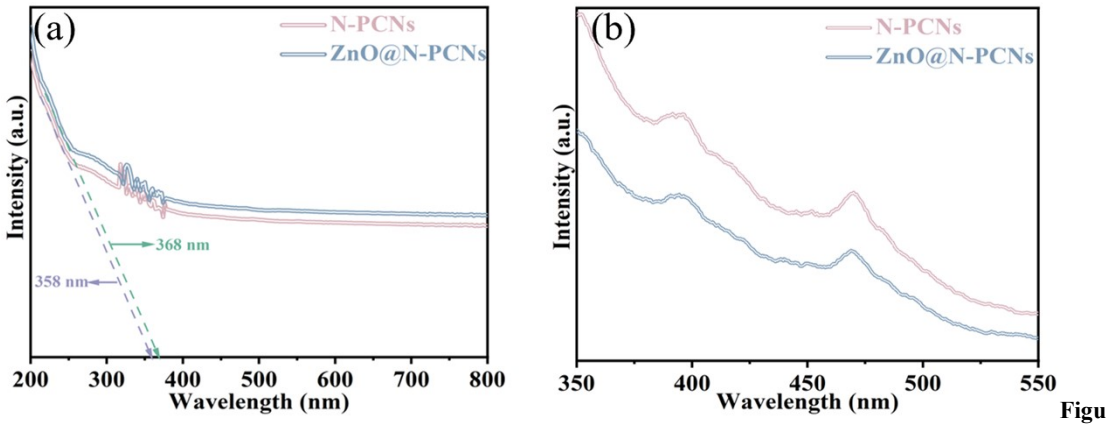

Figure S5. (a) UV-vis spectra and (b) PL spectra of ZnO@N-PCNs and N-PCNs.

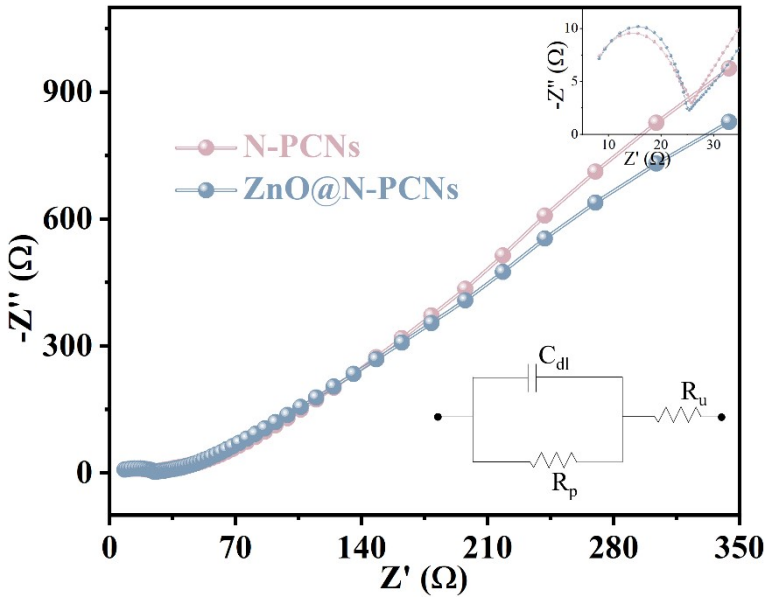

Figure S6. EIS curves of the as-prepared ZnO@N-PCNs and N-PCNs.

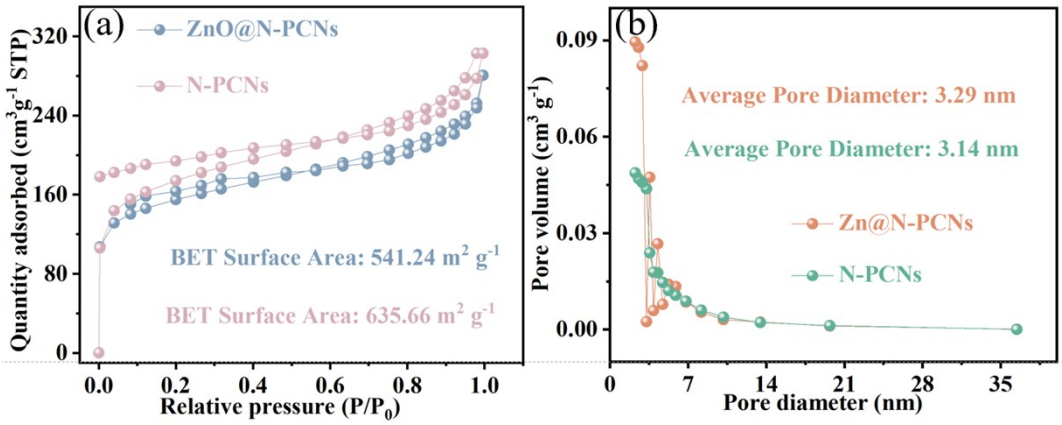

Figure S7. (a) The N_2 adsorption-desorption isotherm of the ZnO@N-PCNs; (b) The pore-size distribution curve of ZnO@N-PCNs.

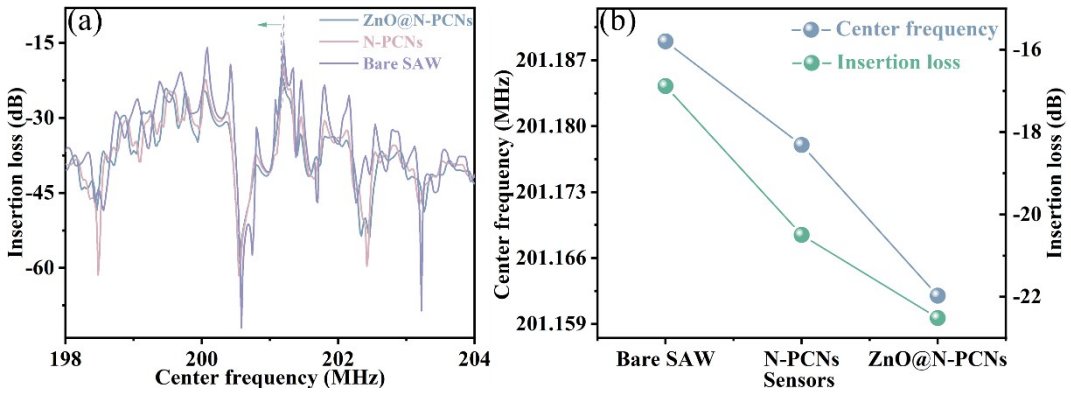

Figure S8. (a) Measured resonant frequency and insertion loss characteristics of the proposed devices of ZnO@N-PCNs, N-PCNs, and bare SAW sensors, (b) summary of the relation between the center frequency and the insertion loss of the as prepared devices.

2. Computational details

DFT calculations were generally performed using the Vienna Ab initio Simulation Package (VASP), where the generalized gradient approximation (GGA) and Perdew-Becke-Ernzerh (PBE) were used to describe electron exchange interactions. The maximal atomic force and total energy tolerances for the structural relaxation are within 1.0×10^{-6} eV and 0.01 eV/Å, respectively. Additionally, a $3 \times 3 \times 1$ k mesh is used, and 600 eV is the kinetic energy cutoff. A layer of vacuum with a thickness of at least 15 Å in the z-direction is adopted to avoid interaction between two adjacent slabs.

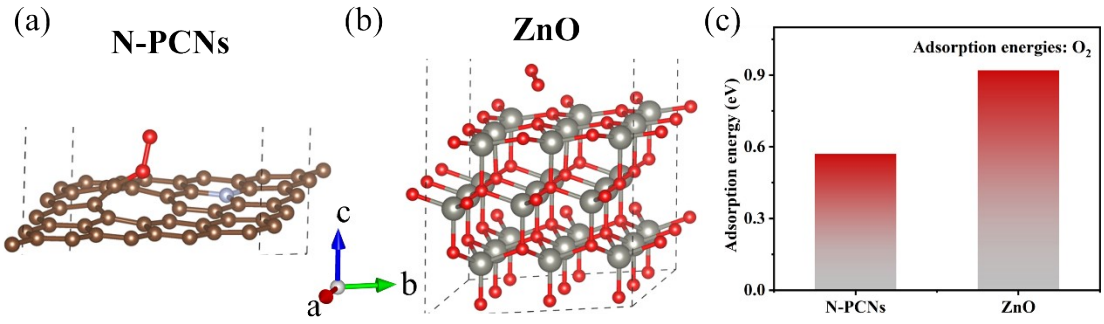

Figure S9. The favorable configurations of O_2 adsorption on (a) N-PCNs and (b) ZnO; (c) The adsorption energies of O_2 on different sensing materials.

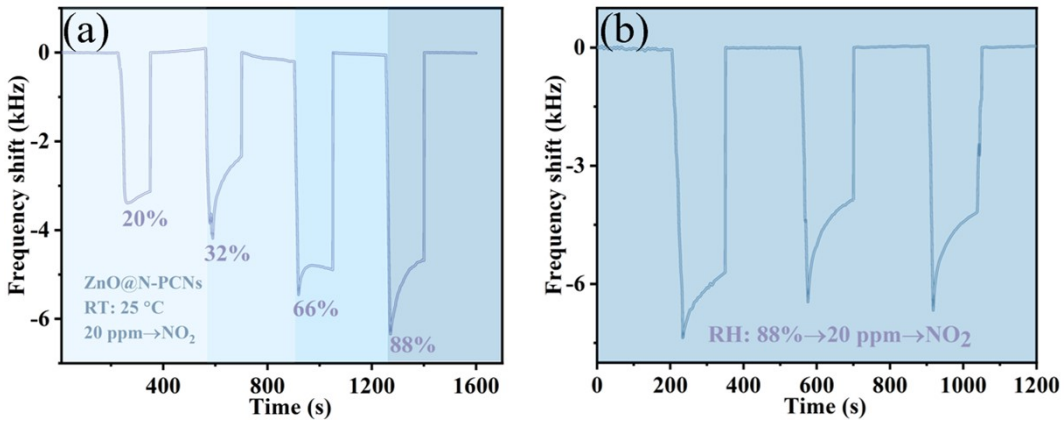

Figure S10. (a) The frequency shifts of prepared SAW sensors under different humidities; (b) Repeatability testing of the SAW sensor under high humidity.

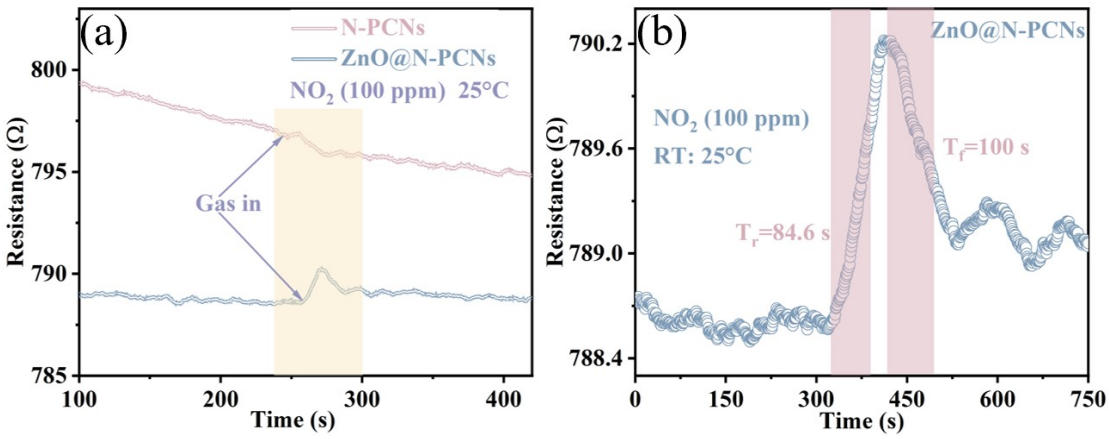

Figure S11. (a) Changes in impendence of the sensors when exposed to NO_2 atmosphere; (b) Response and recovery times of the ZnO@N-PCNs SAW sensor.

Table S1. NO_2 gas sensing properties of different sensing materials coated on SAW sensor.

Sensitive materials	Operating temperature	Concentration(ppm)	Frequency shift(kHz)	Response/recovery time(s)	Ref.
ZnO nanobelt	160℃	10	3.5	~90/140	2
PbS QDs	RT	10	-2.2	487/302	3
GO	RT	50	0.32	~225/321	4
SiO_2-TiO_2	RT	10	0.2	–	5
Polypyrrole	RT	100	2.5	~143/250	6
ZnO@N-PCNs	**RT**	**20**	**-4.4**	**9.9/-**	**This work**

Reference

1 G, Ren, B. Huang, C. Li, C. Lin, and Y. Qian, Facile and template-free strategy to construct N, P co-doped porous carbon nanosheets as a highly efficient electrocatalyst towards oxygen reduction reaction, *J. Electroanal. Chem.*, 2020, 877, 114732.

2 A. Z. Sadek, W. Wlodarski, K. Kalantar, D. A. Powell, H_2 and NO_2 Gas Sensors with ZnO Nanobelt Layer on 36° $LiTaO_3$ and 64° $LiNbO_3$ SAW Transducers, Proceedings of the Fourth IEEE Sensors 2005 Conference, RMIT University, 2005, 1343–1346.

3 M. Li, H. Kan, S. Chen, X. Feng, H. Li, C. Li, C. Fu, A. Quan, H. Sun, J. Luo, X. Liu, W. Wang, H. Liu, Q. Wei, and Y. Fu, Colloidal quantum dot-based surface acoustic wave sensors for NO_2-sensing behavior, *Sens. Actuators, B*, 2019, **287**, 241–249.

4 Q. B. Tang, Y. J. Guo, Y. L. Tang, G. D. Long, J. L. Wang, D. J. Li, X. T. Zu, J. Y. Ma, L. Wang, H. Torun,

and Y. Q. Fu, Highly sensitive and selective Love mode surface acoustic wave ammonia sensor based on graphene oxides operated at room temperature, *J. Mater. Sci.*, 2019, **54**, 11925–11935.

5 Y. J. Guo, G. D. Long, Y. L. Tang, J. L. Wang, Q. B. Tang, X. T. Zu, J. Y. Ma, B. Du, H. Torun, and Y. Q. Fu, Surface acoustic wave ammonia sensor based on SiO_2-SnO_2 composite film operated at room temperature, *Smart Mater. Struct.*, 2020, **29**, 095003.

6 L. A. Mashat, H. D. Tran, W. Wlodarski, R. B. Kaner, and K. K. Zadeh, Polypyrrole nanofiber surface acoustic wave gas sensors, *Sens. Actuators, B*, 2008, **134**, 826–831.